Chinese Chemical Letters 36 (2025) 110520

Contents lists available at ScienceDirect

Chinese Chemical Letters

journal homepage: www.elsevier.com/locate/cclet

Boron cluster-based TADF emitter *via* through-space charge transfer enabling efficient orange-red electroluminescence

Xiao Yu[a,1], Dongyue Cui[b,1], Mengmeng Wang[a], Zhaojin Wang[c], Mengzhu Wang[d], Deshuang Tu[a], Vladimir Bregadze[e], Changsheng Lu[a], Qiang Zhao[d], Runfeng Chen[b,*], Hong Yan[a,*]

[a] State Key Laboratory of Coordination Chemistry, Jiangsu Key Laboratory of Advanced Organic Materials, School of Chemistry and Chemical Engineering, Nanjing University, Nanjing 210023, China
[b] Key Laboratory for Organic Electronics and Information Displays & Jiangsu Key Laboratory for Biosensors, Institute of Advanced Materials (IAM), Jiangsu National Synergistic Innovation Center for Advanced Materials (SICAM), Nanjing University of Posts & Telecommunications, Nanjing 210023, China
[c] Key Laboratory for Advanced Technology in Environmental Protection of Jiangsu Province, Yancheng Institute of Technology, Yancheng 224051, China
[d] College of Electronic and Optical Engineering & College of Flexible Electronics (Future Technology), Nanjing University of Posts & Telecommunications, Nanjing 210023, China
[e] A.N.Nesmeyanov Institute of Organoelement Compounds (INEOS), Russian Academy of Sciences, Moscow 119991, Russia

ARTICLE INFO

Article history:
Received 25 July 2024
Revised 24 August 2024
Accepted 29 September 2024
Available online 30 September 2024

Keywords:
Thermally activated delayed fluorescence
Through-space charge transfer
Carborane
Boron clusters
Organic light-emitting diodes

ABSTRACT

Thermally activated delayed fluorescence (TADF) materials driven by a through-space charge transfer (TSCT) mechanism have garnered wide interest. However, access of TSCT-TADF molecules with long-wavelength emission remains a formidable challenge. In this study, we introduce a novel V-type D-A-D-A' emitter, Trz-*m*CzCbCz, by using a carborane scaffold. This design strategically incorporates carbazole (Cz) and 2,4,6-triphenyl-1,3,5-triazine (Trz) as donor and acceptor moieties, respectively. Theoretical calculations alongside experimental validations affirm the typical TSCT-TADF characteristics of this luminogen. Owing to the unique structural and electronic attributes of carboranes, Trz-*m*CzCbCz exhibits an orange-red emission, markedly diverging from the traditional blue-to-green emissions observed in classical Cz and Trz-based TADF molecules. Moreover, bright emission in aggregates was observed for Trz-*m*CzCbCz with absolute photoluminescence quantum yield (PLQY) of up to 88.8%. As such, we have successfully fabricated five organic light-emitting diodes (OLEDs) by utilizing Trz-*m*CzCbCz as the emitting layer. It is important to note that both the reverse intersystem crossing process and the TADF properties are profoundly influenced by host materials. The fabricated OLED devices reached a maximum external quantum efficiency (EQE) of 12.7%, with an emission peak at 592 nm. This represents the highest recorded efficiency for TSCT-TADF OLEDs employing carborane derivatives as emitting layers.

Organic light-emitting materials have attracted huge attention because of their promising applications in future lighting, displays and medicine [1–4]. Recently, thermally activated delayed fluorescence (TADF) molecules which can harvest both singlet and triplet excitons become the focus in science and industry [5–9]. For the TADF mechanism, the ambient thermal energy is instrumental in promoting efficient reverse intersystem crossing (RISC) from the triplet (T_1) to the singlet (S_1) excited states. This process is facilitated by the small energy gap (ΔE_{ST}) between these states, typically <0.25 eV, which is conducive to an effective RISC process. The RISC process generally unfolds on the microsecond (μs) scale [10]. Since this foundational discovery, TADF-active materials have been extensively developed and optimized, which further significantly improve organic light-emitting diodes (OLED) performances [11–13]. The mechanisms underlying TADF are primarily categorized into through-bond charge transfer (TBCT) and through-space charge transfer (TSCT), which are pivotal for the practical implementation of TADF in various applications.

As TBCT molecules, the donor (D) and acceptor (A) units are interconnected *via* conjugated linkages, allowing π-electron delocalization to extend along σ-bonds [14]. The dihedral angle between D and A units critically influences the charge distribution.

* Corresponding authors.
E-mail addresses: iamrfchen@njupt.edu.cn (R. Chen), hyan1965@nju.edu.cn (H. Yan).
[1] These authors contributed equally to this work.

https://doi.org/10.1016/j.cclet.2024.110520
1001-8417/

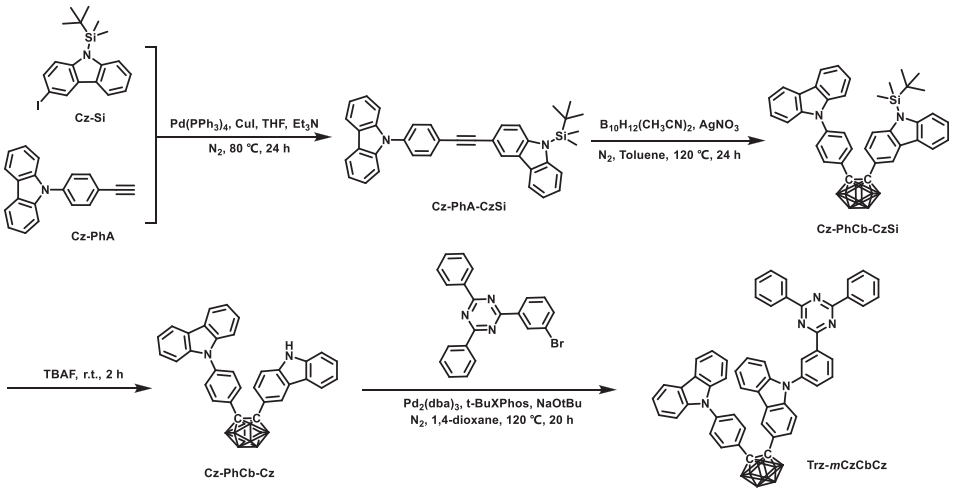

Scheme 1. Synthesis of Trz-*m*CzCbCz.

[15–17]. A larger dihedral angle correlates with well spatial separation between the highest occupied molecular orbital (HOMO) and the lowest unoccupied molecular orbital (LUMO), which means a smaller ΔE_{ST}. In comparison, TSCT occurs in spatially isolated molecules or molecular fragments, where the D/A moieties are close to each other without direct chemical bonding [18–20]. Emitters featuring TSCT have shown considerable promise in the design of photoelectric materials [21–25]. Emitters designed with TSCT characteristics are distinguished by several features [20,26–31]: (1) The spatial separation between D and A units facilitates the spatially separated frontier molecular orbitals and simultaneously enhances the radiative decay rates. (2) The molecular architecture mitigates the reduction in photoluminescence quantum yield (PLQY) typically caused by intermolecular π-π interactions in solid-state environments. (3) The inherent conformational flexibility of TSCT molecules renders them to respond to external stimuli, enhancing their utility in dynamic applications. (4) The structural freedom inherent in the TSCT design expands the diversity of TADF materials. (5) The reduction in electronic coupling between D and A units in TSCT molecules generally results in a larger energy gap. Presently, the exploration of TSCT molecules for photoelectric applications is garnering significant interest. Nonetheless, the development of high-efficiency TADF emitters that leverage the TSCT effect has predominantly been confined to the blue-to-green spectral region [32–34].

Carboranes (*i.e.*, $C_2B_{10}H_{12}$) are icosahedral clusters with three-dimensional (3D) delocalization, bulky size (~1 nm), high thermal stability, and special electronic properties [35,36]. The carborane group exhibits strong electron-withdrawing ability *via* C-substitution and weak electron-donating property *via* B-substitution. Due to these special properties, luminescent materials employing *o*-carborane as a functional unit usually exhibit striking photoelectric properties, including stimuli-response [37–42], excitation-dependent emission [43], multi-emission [44–48], circularly polarized luminescence [49], and so on [50–53]. Particularly, carboranes effectively mitigate aggregation-caused quenching effects, resulting in noteworthy solid-state luminescence [54–58]. So far, carboranes have been widely utilized in sensing [59,60], biological imaging [61–63], and photovoltaics [64]. However, carborane-based TADF emitters and OLEDs are rarely reported [65–69]. In 2016, carborane-based OLED featuring a TSCT-TADF process was firstly reported [70]. Nowadays, carborane turned out to be a promising scaffold to realize a TSCT process because of the unique non-conjugated 3D structure. Since the strong electron-withdrawing ability, carborane may fine-tune the energy levels of luminogens, and is identified as a promising candidate for designing long-wavelength luminogens spanning from orange-red to near-infrared (NIR) regions [39,49,56,57].

In this context, a non-symmetric D-A-D-A' type emitter Trz-*m*CzCbCz is designed and synthesized, in which carbazole (Cz) is employed as a D unit, 2,4,6-triphenyl-1,3,5-triazine (Trz) and carborane are selected as A and A' groups (Scheme 1). Note that the terminal and internal Cz are denoted as Cz_1, Cz_2, respectively. Theoretical calculations show that this molecule involves a TSCT process between Cz_1 and Trz groups. In addition, due to the strong electron-withdrawing property of carborane, the energy level of HOMO and LUMO is considerably reduced. As a result, Trz-*m*CzCbCz has been experimentally confirmed with distinct TADF property. Moreover, Trz-*m*CzCbCz in a doped-film state exhibits orange-red emission with a PLQY of up to 88.8%. By employing this molecule as an emitter, five OLED devices have been manufactured, among which the maximum electroluminescent wavelength of 592 nm and a maximum external quantum efficiency (EQE) of 12.7% have been achieved. To the best of our knowledge, this is the highest efficiency of carborane-based TSCT-type OLED. Through the use of the advantages of carborane, the current research provides a novel strategy for the development of TSCT-TADF molecules featuring orange or red emissions.

Cz and Trz are popular building blocks for constructing TADF emitters owing to a wide range of sources, excellent charge-transporting ability, and good thermal and electrochemical stability. Emitters employing Cz/Trz have been mainly limited to the blue-to-green emission. Therefore, selecting both as D/A segments can not only guarantee good photophysical properties and stability of the luminogen, but also highlight the ability of carborane which can affect wavelength. The introduction of Cz_2 between Cz_1 and Trz groups is expected to regulate the LUMO and construct a suitable conformation for TSCT between the Cz_1 and Trz groups. The synthetic route of Trz-*m*CzCbCz is shown in Scheme 1. Initially, the Sonogashira cross-coupling reaction between Cz-Si [71] and Cz-PhA [72] afforded the precursor Cz-PhA-CzSi, which subsequently reacted with $B_{10}H_{12}(CH_3CN)_2$ to give the carborane derivative Cz-PhCb-CzSi. By the desilylation reaction, the precursor Cz-PhCb-Cz was prepared. Then, Trz-*m*CzCbCz was obtained from the Buchwald-Hartwig reaction between Cz-PhCb-Cz and 2-(3-bromophenyl)-4,6-diphenyl-1,3,5-triazine. ^{1}H, ^{13}C, and ^{11}B NMR spectroscopy were used to characterize the structure. The details of the synthesis and characterization data are provided in the Supporting information.

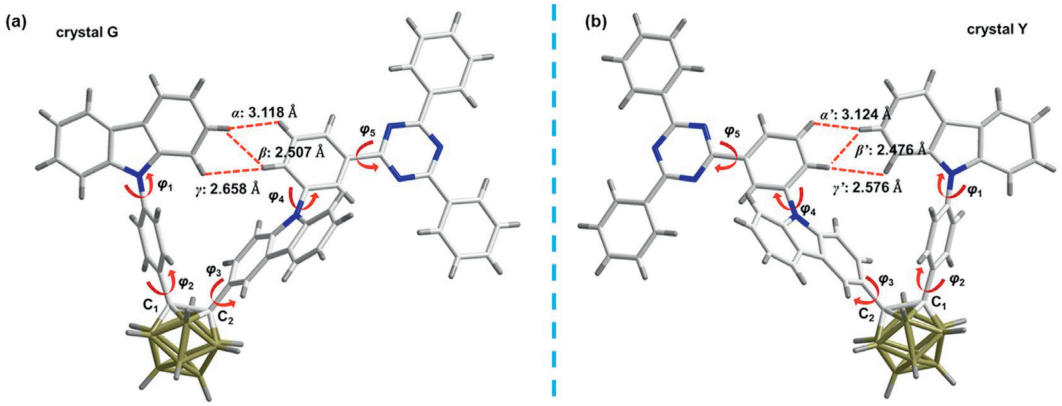

Fig. 1. The selected chemical bonds and dihedral angles of (a) crystal G and (b) crystal Y.

Table 1
Photophysical data of Trz-*m*CzCbCz in different states at room temperature.

	Toluene	Neat film	Powder	Crystal G	Crystal Y	mCP film	DBFPO film
λ_{em} (nm)	582[a]	555[a]	524	533	553	583 [a]	591 [a]
τ (ns)	15.1/621.6[a]	28.8/1200[a]	7.5/38.7	6.6/52.1	6.4/85.8	10.7/8700 [a]	9.9/9600 [a]
PLQY (%)	5.3	65.3	51.8	40.5	25.4	88.8	82.6

[a] Measured in N_2 atmosphere.

Trz-*m*CzCbCz possesses good thermal property with a decomposition temperature of 491 °C (5% weight loss, Fig. S1 in Supporting information). The HOMO energy level determined from electrochemical data is −6.8 eV (Fig. S2 in Supporting information). The energy gap (E_g) is 3.7 eV estimated from the onset of the UV–vis spectrum. The LUMO energy level is −3.1 eV calculated by the formula LUMO = HOMO + E_g. Compared with the molecules based on Cz and Trz groups in literature [73], Trz-*m*CzCbCz possesses deeper energy levels of HOMO and LUMO, which should be caused by the electron-withdrawing property of the carborane group.

The single crystal X-ray diffraction analysis for Trz-*m*CzCbCz was performed. The crystal structures including packing structure diagrams, crystallographic data, and selected chemical bonds and dihedral angle data are shown in Fig. 1, Table 1, Tables S1-S3 and Figs. S3-S5 (Supporting information). Interestingly, two types of crystals of Trz-*m*CzCbCz were obtained, which grew from the mixed solvents of DCM/MeOH showing green (G) and yellow (Y) emissions. During the crystal growth, crystal G appeared first, which could become yellow emission by heating or grinding, thus crystals G and Y should be kinetic and thermodynamic products, respectively. Both crystals G and Y exhibit a V-type shape. No obvious differences for the selected angles φ_1-φ_5 and the C_1–C_2 bond lengths were observed (Tables S2 and S3 in Supporting information), and the packing diagrams of crystals G and Y are mirror-symmetric (Fig. 1). The dihedral angles between the Cz_1 and Trz (φ_6) for crystals G and Y are 42.5° and 41.7°, respectively, which leads to an edge-to-face alignment of the D/A counterpart. In addition, three intramolecular C–H···H–C interactions between D and A units are observed for both crystals (Figs. 1a and b), which is beneficial for the efficient TSCT process. Moreover, the bonding distance between C–H···H–C interactions, for instance γ and γ' is 0.082 Å, which may be the reason for the emissive difference between crystals G and Y.

To gain insight into the electronic structure of Trz-*m*CzCbCz, density function theory (DFT) and time-dependent DFT (TD-DFT) simulations were carried out. For the S_1 state, the "hole" is distributed on the Cz_1 and the adjacent phenylene, while the "particle" is located on the Trz unit (Fig. 2). The calculation predicts the TSCT process of Trz-*m*CzCbCz in the excited state. The energy levels of S_1 and T_1 states are 2.73 eV and 2.56 eV, respectively. Therefore the calculated ΔE_{ST} is 0.17 eV, indicating that an efficient RISC process could occur between S_1 and T_1.

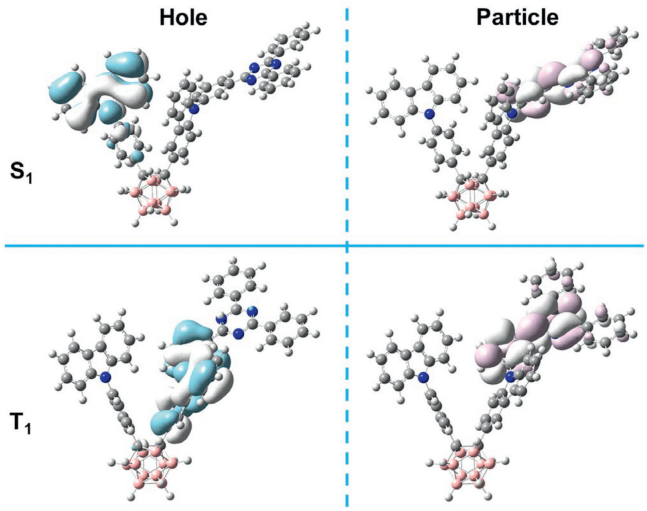

Fig. 2. Frontier orbital distributions of Trz-*m*CzCbCz.

The UV–vis spectrum of Trz-*m*CzCbCz in the neat-film state is shown in Fig. 3a. In the absorption spectra, the bands at 244 nm and 277 nm are mainly attributed to the π-π^* transitions of Cz units, and the shoulder around 326 nm is attributed to the charge transfer transition. Moreover, we also measured the UV–vis spectrum in toluene (Fig. S6 in Supporting information). The two bands at 325 and 338 nm may be attributed to the π-π^* transition. The shoulder around 355 nm may be attributed to the charge transfer transition. Generally, the weakest absorption peak should be located at 450 nm or longer wavelengths in orange-red TSCT molecules. However, many studies found that the weakest absorption peak is blue-shift in carborane-based orange-red TSCT molecules [53,54].

The fluorescence and phosphorescence spectra of Trz-*m*CzCbCz were measured in dilute toluene solution (10^{-5} mol/L) as illustrated in Fig. 3b. At 298 K, the spectrum shows an unstructured

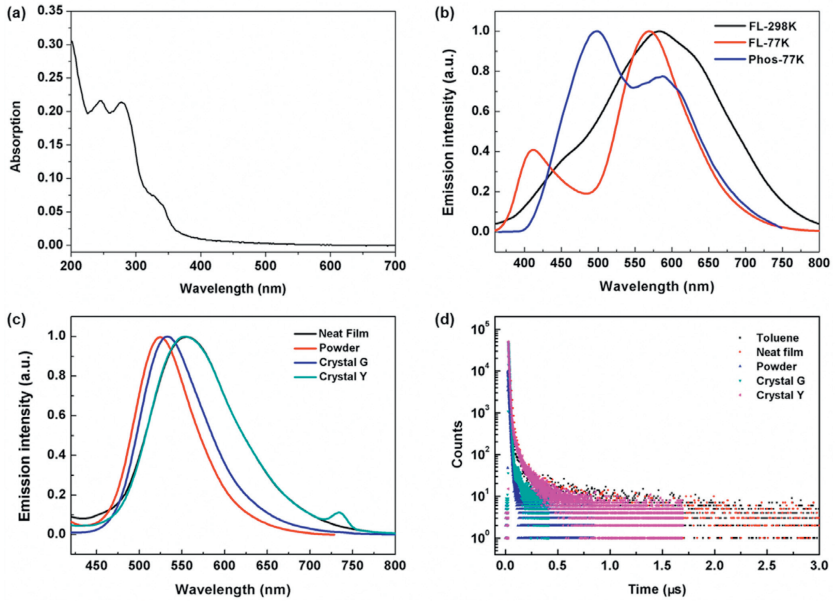

Fig. 3. (a) UV–vis spectrum of Trz-*m*CzCbCz at room temperature in neat film. (b) The fluorescence and phosphorescence spectra of Trz-*m*CzCbCz in dilute toluene (10^{-5} mol/L). (c) The photoluminescence spectra of Trz-*m*CzCbCz in aggregate states. (d) Transient PL spectra of Trz-*m*CzCbCz at room temperature.

and broad profile, and the maximum emission peak (λ_{em}) is located at 582 nm with a shoulder around 450 nm. According to literature [74], the shoulder is caused by the TBCT process from Cz_2 to Trz. At 77 K, the fluorescence spectrum exhibits obvious dual emissions at 410 nm and 568 nm, which suggests that the TBCT process is enhanced. The phosphorescence spectrum also shows two emission peaks at 420 and 570 nm. From the onsets of the fluorescence and phosphorescence spectra, ΔE_{ST} of Trz-*m*CzCbCz is estimated to be 0.0975 eV, which is small enough for a RISC process. Then, we measured the transient decay spectrum in degassed toluene at room temperature (Fig. 3d and Table 1). The lifetimes of prompt decay (τ_{PF}) and delay decay components (τ_{DF}) are estimated to be 15.1 ns and 621.6 ns, respectively.

To obtain additional insights into the photophysical properties of Trz-*m*CzCbCz, its emission spectra in neat film, powder and crystals G and Y were also measured (Fig. 3c), of which λ_{em} are located at 555 nm, 524 nm, 533 nm and 553 nm, respectively. In these aggregate states, no shoulders in the high-energy region were observed, and the full width at half maximum (FWHM) are obviously decreased compared with those in toluene, indicating a dominant TSCT process. Transient PL decay curves of these aggregate states exhibit two-exponential decay, as shown in Fig. 3d and Table 1. The τ_{PF} and τ_{DF} values of Trz-*m*CzCbCz in the neat film are 28.8 ns and 1.2 μs, respectively, which manifests the typical TADF characteristic. However, the lifetimes of powder and crystals are all in the nanosecond scale owing to the π-π stacking.

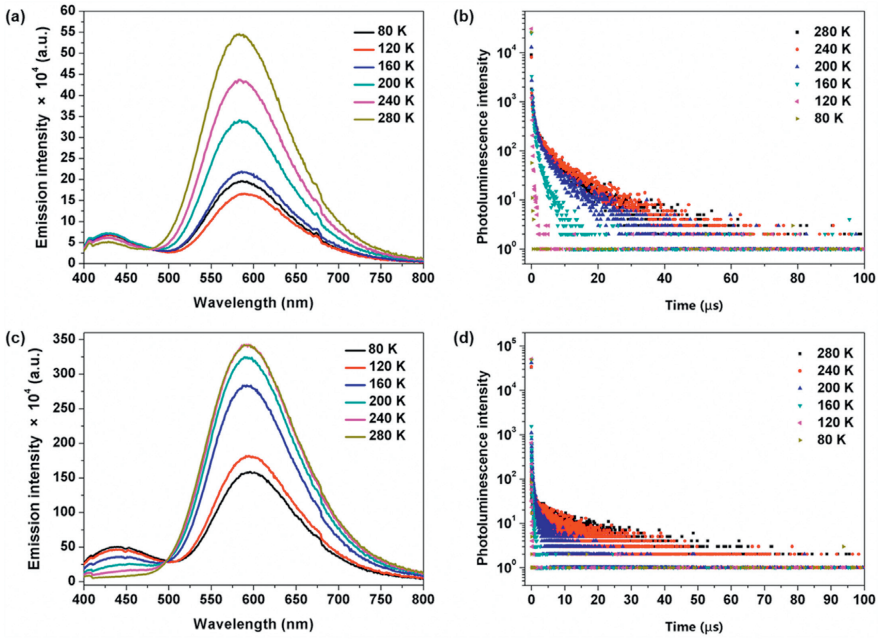

Fig. 4. (a) Temperature-dependent PL spectra of mCP doped-film. (b) Transient PL decay curves of mCP doped-film. (c) Temperature-dependent PL spectra of DBFPO doped-film. (d) Transient PL decay curves of DBFPO doped-film.

The PLQY of Trz-*m*CzCbCz in the dilute toluene solution is relatively low at 5.3%. This reduced efficiency can be ascribed to non-radiative decay processes, predominantly influenced by vibrations of the carborane C_1–C_2 bond in solution, as documented in previous studies [61]. In stark contrast, in aggregated states the PLQYs exhibit a substantial increase, reaching up to 65.3%. This significant enhancement in quantum yield indicates the potential of Trz-*m*CzCbCz as a luminescent material for application in OLEDs.

To further investigate the TADF characteristic and evaluate the potential as the emission layer of OLED, we measured the temperature-dependent PL spectra and transient PL decay curves of Trz-*m*CzCbCz in the doped films (20 wt%). Here, 9,9′-(1,3-phenylene)bis-9*H*-carbazole (mCP) and dibenzo[*b*,*d*]furan-2,8-diylbis(diphenylphosphine oxide) (DBFPO) were selected as the host materials (Fig. 4). With the temperature decreased from 280 K to 80 K, the Trz-*m*CzCbCz in mCP film and DBFPO film exhibits the reduced PL intensity with λ_{em} at 583 and 591 nm, respectively. The slight red shift of λ_{em} in different hosts is caused by the higher polarity of hosts. Note that, λ_{em} in doped films have a significant red-shift compared to neat film, which may be caused by the formation of exciplex between the emitters and host molecules. Besides, the DBFPO doped film shows an obvious shoulder around 430 nm in PL spectra, which suggests that the host material may affect the ratio between TBCT and TSCT. The τ_{DF} values of Trz-*m*CzCbCz doped in mCP and DBFPO are 8.7 μs and 9.6 μs, respectively. As the temperature is decreased, the delayed components of the transient PL spectra are decreased, which demonstrates the TADF characteristic in both films. Moreover, Trz-*m*CzCbCz in the mCP host emerges a higher ratio of delay decay component and a shorter τ_{DF}. This result clarifies that the mCP host would be conducive to a small ΔE_{ST} and effective RISC process compared to DBFPO. Exhilaratingly, Trz-*m*CzCbCz exhibits high PLQY of 88.8% and 82.6% in mCP and DBFPO host, respectively. Thus, we can employ both as host materials to construct OLED devices.

The above excellent photophysical properties of Trz-*m*CzCbCz inspired us to investigate electroluminescence (EL) performances. Due to the deep HOMO energy, we selected DBFPO as the host material and designed the device structure as shown in Fig. 5a. The structures of the materials involved in these devices are shown in Fig. 5b. The devices A-D correspond to non-doped, 10 wt%, 20 wt% and 30 wt% concentration of Trz-*m*CzCbCz, respectively. The detailed device data are presented in Fig. 5 and Table 2. The shoulders of PL spectra are absent in EL spectra, indicating that the TSCT

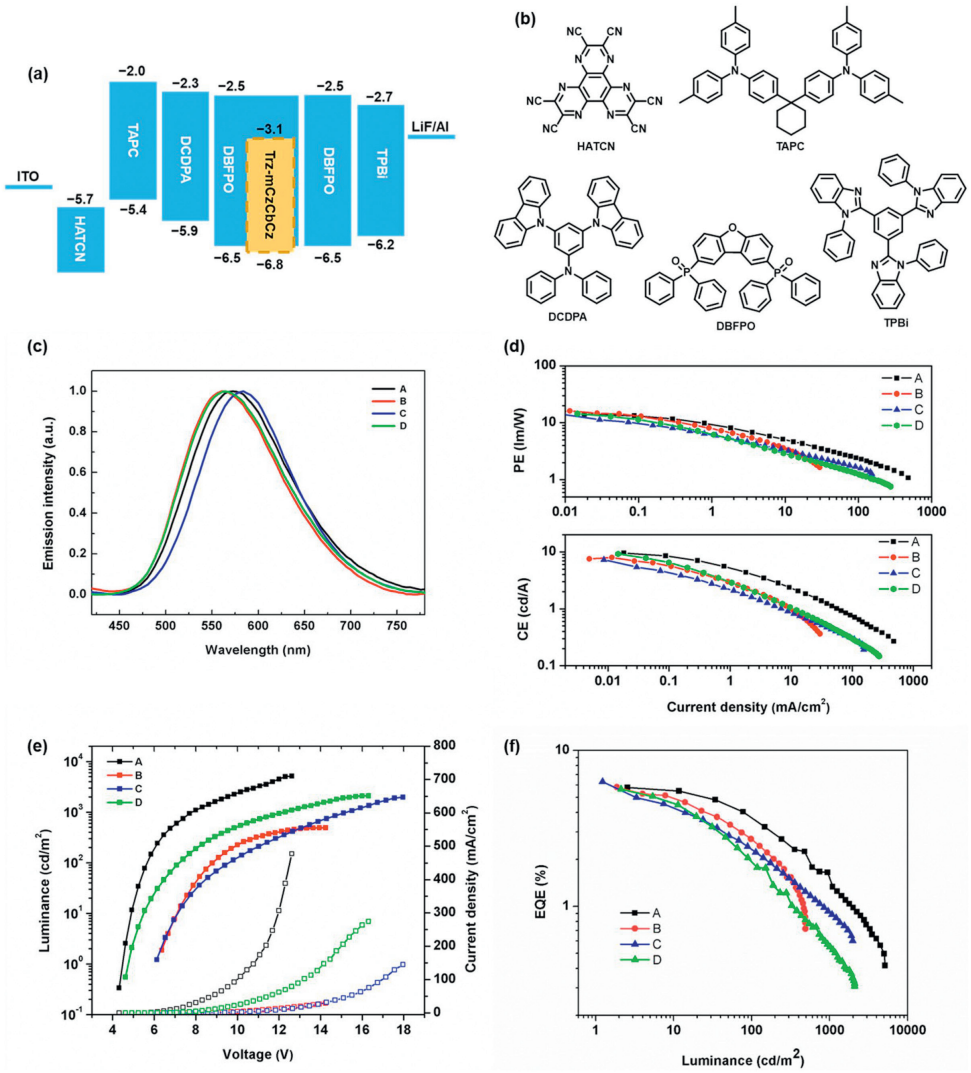

Fig. 5. (a) Schematic diagram and energy level of devices A-D. (b) Molecular structures of the compounds used in the devices. (c) Normalized EL spectra at 10 V of these devices. (d) Power efficiency (PE), current efficiency (CE) *versus* luminance of these devices. (e) Luminance–voltage-current density (*L-V-J*) curves. (f) EQE *versus* luminance of these devices.

Table 2
Device performances of Trz-*m*CzCbCz.

Device	V_{on} (V)	J_{max} (mA/cm^2)	CE_{max} (cd/A)	PE_{max} (lm/W)	EQE_{max} (%)	λ_{max} (nm) @10V	L_{max} (cd/m^2)	CIE[a] 1931@10V
A	4.31	477.44	14.05	9.56	5.77	572	5158	(0.48, 0.49)
B	6.36	29.66	16.21	8.00	5.81	564	490	(0.45, 0.49)
C	6.12	145.07	14.25	7.30	6.29	584	1977	(0.49, 0.47)
D	4.62	274.62	14.45	9.22	5.64	564	2091	(0.45, 0.50)
E	15.22	211.55	29.95	0.01	12.70	592[a]	2055	(0.51, 0.47)[b]

[a] CIE denotes Commission Internationale de L'Eclairage.
[b] Measured at 20 V.

process is dominant in the EL process (Fig. 5c). Besides, the doping concentration also affects the current efficiency (CE), power efficiency and the *J-V-L* characteristics (Figs. 5d and e). Non-doped device A shows a small turn-on voltage of 4.3 V, indicating a good charge injection and transport. However, device C shows the maximum external quantum efficiency (EQE) of 6.29%. EQE of all these devices exceeds 5% (Fig. 5f). To obtain a higher value of EQE, we adopted mCP as a host material and designed device E with a structure as shown in Fig. 6a. Because the energy levels of mCP and DBFPO are different, it is necessary to design different structures to obtain better performance. So, the structure of device E is different from that of devices A-D. The concentration of Trz-*m*CzCbCz in device E is 20 wt%. As a result, device E demonstrates a much higher EQE of 12.7% owing to the more efficient RISC process of mCP doped-film. This represents the best performance among the TSCT-type OLEDs based on carborane derivatives. However, the turn-on voltage is 15.2 V, and the PE value is 0.01 lm/W (Fig. 6 and Table 2).

In summary, a novel V-type D-A-D-A' TADF emitter of Trz-*m*CzCbCz featuring a TSCT characteristic has been designed and synthesized. The donor/acceptor units of Cz/Trz as well as the unique carborane scaffold endow the molecule with special structural and electronic properties. This leads to the excellent TSCT-type TADT emitter exhibiting an orange-red emission with PLQY up to 88.8%. The fabricated OLED device using Trz-*m*CzCbCz as an emitter reaches an EQE of 12.7% with a long-wavelength emission at 592 nm. This is the highest EQE among the boron cluster-based TSCT-TADF molecule.

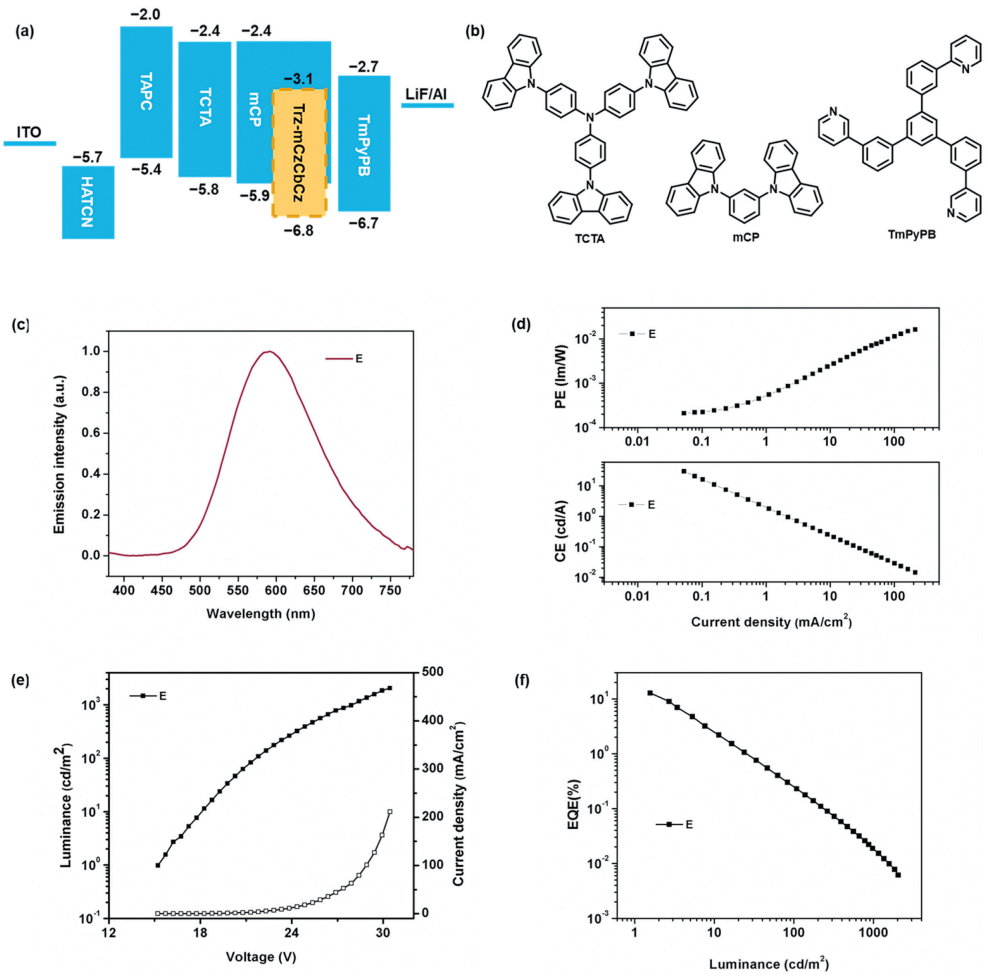

Fig. 6. (a) Schematic diagram and energy level of device E. (b) Molecular structures of the compounds used in the device E. (c) Normalized EL spectrum at 20 V of device E. (d) PE, CE *versus* luminance of device E. (e) *L-V-J* curves of device E. (f) EQE *versus* luminance of device E.

Declaration of competing interest

The authors declare that they have no known competing financial interests or personal relationships that could have appeared to influence the work reported in this paper.

CRediT authorship contribution statement

Xiao Yu: Writing – review & editing, Writing – original draft, Methodology, Investigation, Formal analysis, Data curation, Conceptualization. **Dongyue Cui:** Visualization, Investigation, Data curation. **Mengmeng Wang:** Investigation, Data curation. **Zhaojin Wang:** Writing – review & editing, Conceptualization. **Mengzhu Wang:** Data curation. **Deshuang Tu:** Writing – review & editing, Formal analysis, Conceptualization. **Vladimir Bregadze:** Supervision, Funding acquisition. **Changsheng Lu:** Supervision, Project administration. **Qiang Zhao:** Data curation. **Runfeng Chen:** Visualization, Supervision, Funding acquisition, Data curation. **Hong Yan:** Writing – review & editing, Validation, Supervision, Project administration, Funding acquisition.

Acknowledgments

This work is supported by the Natural Science Foundation of Jiangsu Province (No. BZ2022007), the National Natural Science Foundation of China (No. 92261202), the Ministry of Science and Technology of the People's Republic of China (No. 2021YFE0114800) and the Ministry of Science and Higher Education of the Russian Federation (No. 075–15–2021–1027). The high-performance computing centers of Nanjing University, the Open Research Fund from Henan Normal University and TaiShan Industrial Experts Programme are also gratefully acknowledged.

Supplementary materials

Supplementary material associated with this article can be found, in the online version, at doi:10.1016/j.cclet.2024.110520.

References

[1] Q. Liao, Q. Li, Z. Li, Adv. Mater. (2023), doi:10.1002/adma.202306617.
[2] M. Dong, A. Lv, X. Zou, et al., Adv. Mater. 36 (2024) 2310663.
[3] P. Fan, Z. Fang, S. Wang, et al., Chin. Chem. Lett. 34 (2023) 107934.
[4] Z. Wei, K. Zhang, C.K. Kim, et al., Chin. Chem. Lett. 32 (2021) 493–496.
[5] X. Dong, S. Shen, Y. Qin, et al., Chin. Chem. Lett. 34 (2023) 108311.
[6] Z. Han, X.Y. Dong, S.Q. Zang, Adv. Opt. Mater. 9 (2021) 2100081.
[7] S.K. Jeon, H.L. Lee, K.S. Yook, J.Y. Lee, Adv. Mater. 31 (2019) 1803524.
[8] M. Zhang, G. Dai, C. Zheng, et al., Chin. Chem. Lett. 33 (2022) 1110–1115.
[9] S. Kiriyama, M. Mamada, K. Goushi, et al., Adv. Funct. Mater. 34 (2024) 2402287.
[10] D.S.M. Ravinson, M.E. Thompson, Mater. Horiz. 7 (2020) 1210–1217.
[11] Yu.C. Liu, C.S. Li, Z.J. Ren, S.K. Yan, M.R. Bryce, Nat. Rev. Mater. 3 (2018) 18020.
[12] G. Hong, X. Gan, C. Leonhardt, et al., Adv. Mater. 33 (2021) 2005630.
[13] X. Hu, Y. Qin, Z. Li, et al., Chin. Chem. Lett. 33 (2022) 4645–4648.
[14] T. Huang, Q. Wang, S. Xiao, et al., Angew. Chem. Int. Ed. 60 (2021) 23771–23776.
[15] Y. Tian, Y.Z. Shi, X.C. Fan, et al., Adv. Opt. Mater. 11 (2023) 2300504.
[16] S. Weissenseel, N.A. Drigo, L.G. Kudriashova, et al., J. Phys. Chem. C 123 (2019) 27778–27784.
[17] X. Jiang, W. Tao, C. Chen, et al., Chem. Sci. 12 (2021) 15928–15934.
[18] Q. Xue, G. Xie, Adv. Opt. Mater. 9 (2021) 2002204.
[19] Y. Xin, Y. Zhu, R. Chi, et al., Adv. Mater. 35 (2023) 2304103.
[20] S.Y. Yang, Y.K. Qu, L.S. Liao, Z.Q. Jiang, S.T. Lee, Adv. Mater. 34 (2021) 2104125.
[21] J. Zhang, D. Li, W. Li, et al., Sci. China Chem. 67 (2024) 1270–1276.
[22] H. Zhu, J. Liu, Y. Wu, et al., J. Am. Chem. Soc. 145 (2023) 11130–11139.
[23] R. Wang, Z. Li, T. Hu, et al., ACS App. Mater. Interfaces 13 (2021) 49066–49075.
[24] J. Liu, Z. Feng, C. Peng, et al., Chin. Chem. Lett. 34 (2023) 107634.
[25] Y.K. Wang, H. Wan, S. Teale, et al., Nature 629 (2024) 586–591.
[26] T. Zhang, Y. Xiao, H. Wang, et al., Angew. Chem. Int. Ed. 62 (2023) e202301896.
[27] W. Yang, C. Xie, T. Chen, et al., Angew. Chem. Int. Ed. 63 (2024) e202402704.
[28] X. Tang, L.S. Cui, H.C. Li, et al., Nat. Mater. 19 (2020) 1332–1338.
[29] B. Li, Z. Yang, W. Gong, et al., Adv. Opt. Mater. 9 (2021) 2100180.
[30] D.Y. Qin, M. Zhang, Y.N. Hu, et al., Chem. Eng. J. 450 (2022) 138174.
[31] F. Chen, J. Hu, X. Wang, et al., Sci. China Chem. 63 (2020) 1112–1120.
[32] X.F. Song, C. Jiang, N. Li, et al., Chem. Sci. 14 (2023) 12246–12254.
[33] C. Jiang, J. Miao, D. Zhang, et al., Research 2022 (2022) 9892802.
[34] H. Tsujimoto, D.G. Ha, G. Markopoulos, et al., J. Am. Chem. Soc. 139 (2017) 4894–4900.
[35] R.N. Grimes, Carboranes, 3rd ed., Elsevier, Oxford, 2016.
[36] N.S. Hosmane, Boron Science: New Technologies and Applications, CRC, Boca Raton, 2011.
[37] J. Ochi, K. Tanaka, Y. Chujo, Angew. Chem. Int. Ed. 59 (2020) 9841–9855.
[38] J.J. Peterson, A.R. Davis, M. Werre, E.B. Coughlin, K.R. Carter, ACS Appl. Mater. Interfaces 3 (2011) 1796–1799.
[39] H. Naito, Y. Morisaki, Y. Chujo, Angew. Chem. Int. Ed. 54 (2015) 5084–5087.
[40] J. Li, C. Yang, X. Peng, et al., J. Mater. Chem. C 6 (2018) 19–28.
[41] A. Saha, E. Oleshkevich, C. Vinas, F. Teixidor, Adv. Mater. 29 (2017) 1704238.
[42] L. Parejo, M. Chaari, S. Santiago, et al., Chem. Eur. J. 27 (2021) 270–280.
[43] H. Yang, H. Liu, Y. Shen, et al., Angew. Chem. Int. Ed. 61 (2022) e202115551.
[44] L. Weber, J. Kahlert, R. Brockhinke, et al., Chem. Eur. J. 18 (2012) 8347–8357.
[45] D. Tu, P. Leong, S. Guo, et al., Angew. Chem. Int. Ed. 56 (2017) 11370–11374.
[46] A. Ferrer-Ugalde, A. González-Campo, C. Viñas, et al., Chem. Eur. J. 20 (2014) 9940–9951.
[47] K.R. Wee, W.S. Han, D.W. Cho, et al., Angew. Chem. Int. Ed. 51 (2012) 2677–2680.
[48] X. Zhao, X. Zhang, X. Li, L. Wu, L. Ji, Chem. Eur. J. 30 (2024) e202401246.
[49] J.H. Huang, Y.J. Liu, Y. Si, et al., J. Am. Chem. Soc. 146 (2024) 16729–16736.
[50] R. Núñez, M. Tarrés, A. Ferrer-Ugalde, F.F. de Biani, F. Teixidor, Chem. Rev. 116 (2016) 14307–14378.
[51] L. Wu, M. Holzapfel, A. Schmiedel, et al., Nat. Commun. 15 (2024) 3005.
[52] X. Wu, J. Guo, Y. Lv, et al., Mater. Chem. Front. 4 (2020) 257–267.
[53] D. Wang, G. Wang, K. Liu, et al., Chin. Chem. Lett. 33 (2022) 2532–2536.
[54] K. Liu, J. Zhang, Q. Shi, et al., J. Am. Chem. Soc. 145 (2023) 7408–7415.
[55] D. Tu, S. Cai, C. Fernandez, et al., Angew. Chem. Int. Ed. 58 (2019) 9129–9133.
[56] F. Aniés, I. Hamilton, C.S.P. De Castro, et al., J. Am. Chem. Soc. 146 (2024) 13607–13616.
[57] C. Lv, Y. Shen, F. Cao, et al., Chem. Eur. J. 29 (2023) e202300049.
[58] X. Wei, M.J. Zhu, Z. Cheng, et al., Angew. Chem. Int. Ed. 58 (2019) 3162–3166.
[59] K. Liu, C. Shang, Z. Wang, et al., Nat. Commun. 9 (2018) 1695.
[60] A.M. Prokhorov, T. Hofbeck, R. Czerwieniec, et al., J. Am. Chem. Soc. 136 (2014) 9637–9642.
[61] C. Shi, H. Sun, X. Tang, et al., Angew. Chem. Int. Ed. 52 (2013) 13434–13438.
[62] L. Zhu, X. Tang, Q. Yu, et al., Chem. Eur. J. 21 (2015) 4721–4730.
[63] X. Li, X. Tong, Y. Yin, et al., Chem. Sci. 8 (2017) 5930–5940.
[64] S. Tan, C. Li, C. Peng, et al., Nat. Commun. 15 (2024) 4136.
[65] R. Yang, Y. Zhou, H. Bian, et al., Chem. Eng. J. 447 (2022) 137432.
[66] T. Lee, J.H. Jang, N.N.T. Nguyen, et al., Adv. Sci. 11 (2024) 2309016.
[67] Z. Wang, J. Zhao, M. Muddassir, R. Guan, S. Tao, Inorg. Chem. 60 (2021) 4705–4716.
[68] Z. Peng, K. Zhang, Z. Huang, et al., J. Mater. Chem. C 7 (2019) 2430–2435.
[69] K. Cheong, S.C. Kim, J.Y. Lee, Dyes Pigments 215 (2023) 111278.
[70] R. Furue, T. Nishimoto, I.S. Park, J. Lee, T. Yasuda, Angew. Chem. Int. Ed. 55 (2016) 7171–7175.
[71] G. Xie, D. Chen, X. Li, et al., ACS Appl. Mater. Interfaces 8 (2016) 27920–27930.
[72] R. Martín, P. Prieto, J.R. Carrillo, et al., J. Mater. Chem. C 7 (2019) 9996–10007.
[73] B. Wex, B.R. Kaafarani, J. Mater. Chem. C 5 (2017) 8622–8653.
[74] D. Liu, D.L. Li, H.H. Meng, Y. Wang, L.Z. Wu, J. Mater. Chem. C 7 (2019) 12470–12481.